8

Regional Climate Change Projections

Authors:
Aurel Florian Moise, Sandeep Sahany, Muhammad Eeqmal Hassim, Chen Chen, Xin Rong Chua, Venkatraman Prasanna, Gerald Lim, Pavan Harika Raavi, Jianjun Yu, Fei Luo

METEOROLOGICAL SERVICE SINGAPORE
Centre for Climate Research Singapore

8.1 Introduction

In the V3 study, the SINGV-RCM has been used to dynamically downscale six sub-selected CMIP6 GCMs over the SEA domain at 8 km horizontal resolution for the historical period (1955-2014) and for the future (2015-2099) under 3 IPCC AR6 global warming scenarios (SSP1-2.6, SSP2-4.5 and SSP5-8.5). This dataset provides the most up-to-date and highest-resolution climate change projections over the SEA region when writing this report.

Although the regional climate change projections were also presented in Chapter 4 of this report using CMIP6 GCM outputs and from the existing literature, results presented in this chapter are based on the 8 km dynamically downscaled projections. The 8 km downscaled projections, although not expected to significantly deviate from the GCM-based projections when it comes to large-scale drivers, are still expected to add a lot more spatial details that cannot be seen from GCM data due to their coarser resolution.

This chapter presents the projections of means and extremes for key climate variables (rainfall, temperature, and relative humidity) over the region and key climate drivers (monsoons, northeast monsoon surges, and ENSO teleconnections). Where appropriate, we also discuss related changes reported in the literature.

8.2 Data and Methodology

This chapter makes use of the historical (1995-2014) and future (mid-century: 2040-2059 and end-century: 2080-2099) 8 km downscaled data over SEA under the 3 SSPs (SSP1-2.6, SSP2-4.5, and SSP5-8.5) to compute projected changes in means and extremes for some key climate variables and some key climate drivers.

Specifically, we compute the mean changes in rainfall and temperature on annual and seasonal timescales (DJF, MAM, JJA, and SON) for mid- and end-century under the 3 SSPs. In addition to the mean, we also compute the changes in temperature and rainfall extremes. For rainfall extremes, we compute changes in the annual maximum 1-day rainfall (RX1day) and annual maximum 5-day rainfall (RX5day), and for temperature extremes, we compute changes in the daily maximum and daily minimum temperatures. We also compute changes in the mean near-surface relative humidity on annual and seasonal timescales for mid- and end-century under the 3 SSPs.

Along with the computation of changes in key climate variables, we also compute changes in some of the important large-scale climate drivers over the region. As mentioned above, we don't expect any significant deviations in the projected changes of the large-scale climate drivers compared to the driving GCMs, except for more spatial details in the downscaled simulations. Specifically, (1) we compute projected changes in the 850hPa winds for each of the seasons mentioned above and, along with the seasonal mean rainfall changes, infer projected changes in the monsoon circulation and associated rainfall, (2) we compute the projected changes in 850 hPa winds and rainfall associated with the northeast monsoon surges, and (3) we present projected changes in the JJA ENSO-rainfall teleconnection by computing correlation coefficient of the 8 km downscaled rainfall with the Nino3.4 SSTs from the driving GCMs.

8.3 Climate Change Projections over the Maritime Continent

In this section, we present the projections of key climate variables (rainfall, temperature, and relative humidity) over the MC from the 8km downscaled projections.

8.3.1 Changes in annual mean rainfall

Figure 8.1 shows the projected changes in the annual mean rainfall over SEA (left panel) and SEA land-only points (right panel) in the mid-century and end-century relative to the historical baseline under the three SSP scenarios. They are also shown in tabular form in Tables 8.1 and 8.2 for readability.

Overall, there is a projected increase in annual mean domain-average rainfall over SEA during the mid and end centuries. Based on the multi-model mean, the end-century change is higher than the mid-century change for each of the scenarios. The inter-scenario spread is larger

during the end of the century (more than 3%) compared to the mid-century (within 1%). The multi-model end-century changes indicate larger increases in domain-average rainfall under scenarios with greater warming, i.e., change under SSP5-8.5 being higher than SSP2-4.5, which in turn is higher than SSP1-2.6.

We also find the projected end-century mean under SSP5-8.5 to be positively skewed due to an outlier model (see the difference between the thin line and the diamond in the left panel of Figure 8.1).

Table 8.1: Projected changes in annual mean rainfall (percent change) - SEA

ANN	Mid-Century (%)		End-Century (%)	
	Mean	Range	Mean	Range
SSP1-2.6	2.1	0.6 to 4.0	2.9	1.3 to 5.7
SSP2-4.5	3.0	1.2 to 4.9	4.0	1.7 to 5.6
SSP5-8.5	2.7	1.0 to 5.3	6.0	0.2 to 15

Table 8.2: Projected changes in annual mean rainfall (percent change) - SEA land regions

ANN	Mid-Century (%)		End-Century (%)	
	Mean	Range	Mean	Range
SSP1-2.6	2.9	0.4 to 4.5	3.9	2.6 to 5.5
SSP2-4.5	4.0	1.6 to 6.6	5.8	3.8 to 7.9
SSP5-8.5	4.0	0.5 to 6.3	8.7	4.2 to 13.4

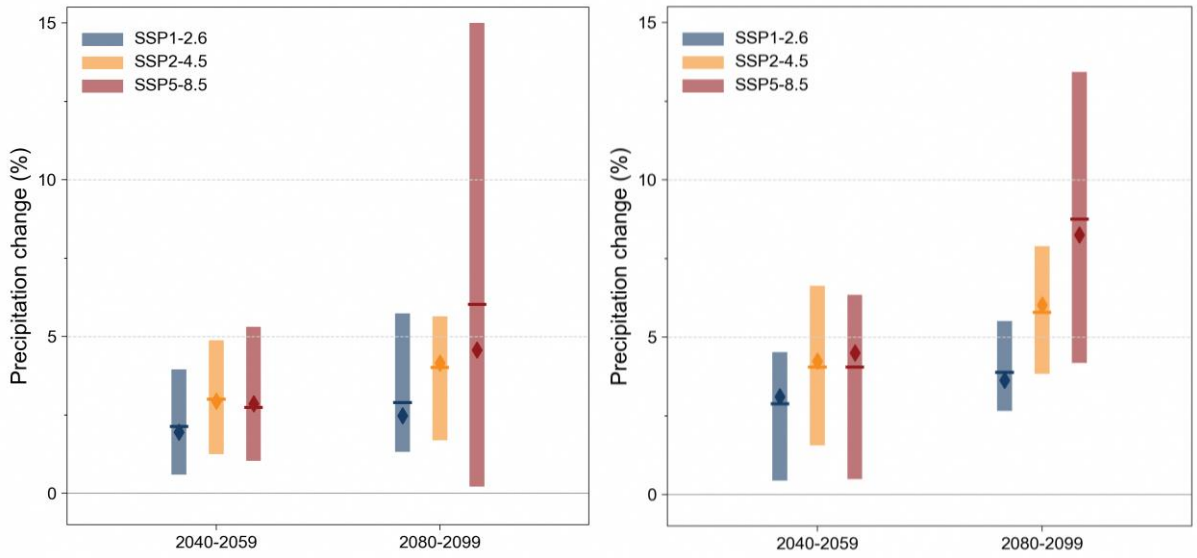

Figure 8.1: Percentage change of annual mean rainfall (pr) over the mid- (2040-59) and end-century (2080-99) period for the six downscaled GCMs (8km) over the SEA domain (left) and SEA land only (right) relative to the historical (1995-2014) baselines. The line and diamond represent the mean and median using the six models, respectively.

Over SEA land points, the projected changes show similar behaviour as the domain average. However, the projected change over land is higher than seen over the entire domain, suggesting higher rainfall changes over land than ocean points. Also, the positive skew seen in the projected end-century mean under SSP5-8.5 is less prominent for SEA land, suggesting that the outlier model projects significant positive changes over the ocean points.

8.3.2 Changes in seasonal mean rainfall

Figure. 8.2 shows the projected changes in the seasonal mean rainfall over SEA land in the mid-century and end century relative to the historical under three SSP scenarios using 8km downscaled GCM simulations. For readability, they are also shown in tabular form in Tables 8.3-8.6 for land. As seen in Figure 8.2, the projected seasonal multi-model mean rainfall is expected to increase both in mid-century and end century across different seasons. During the DJF season, the multi-model seasonal mean rainfall is projected to increase with warming both in mid-century and end century (Table 8.3). In the mid-century, the rainfall changes are similar in SSP1-2.6 (2.8%) and SSP2-4.5 (2.8%) but are larger under SSP5-8.5 (4.6%). In the end century, multi-model rainfall is projected to increase across all scenarios from SSP1-2.6 (2.4%), to SSP2-4.5

(5.0%), to SSP5-8.5(8.0%). The end-century multi-model mean rainfall projections are larger than the mid-century projections in SSP2-4.5 and SSP5-8.5 but slightly smaller in SSP1-2.6.

Table 8.3: Projected changes in seasonal mean rainfall (percent change) - DJF

DJF	Mid-Century (%)		End-Century (%)	
	Mean	Range	Mean	Range
SSP1-2.6	2.8	-1.4 to 5.8	2.4	-0.3 to 10.6
SSP2-4.5	2.8	-3.2 to 5.9	5.0	0 to 10.5
SSP5-8.5	4.6	1.2 to 8.5	8.0	2.5 to 14.5

For the MAM season, the rainfall is projected to increase over the SEA both in mid-century and end century compared to the historical period across all the scenarios. Both in the mid-century and end century, rainfall is projected to increase with warming from SSP1-2.6 to SSP5-8.5. The difference between mid-century and end-century changes is larger in SSP2-4.5 and SSP5-8.5 (~3%) than in SSP1-2.6 (~1.5%).

Table 8.4: Projected changes in seasonal mean rainfall (percent change) - MAM

MAM	Mid-Century (%)		End-Century (%)	
	Mean	Range	Mean	Range
SSP1-2.6	1.3	-3.1 to 4.2	2.8	0.2 to 5.8
SSP2-4.5	2.2	-1.5 to 6.3	5.3	0.4 to 10.6
SSP5-8.5	4.0	-0.9 to 6.6	7.5	0.2 to 16.8

Overall, the seasonal rainfall projections for the JJA seasons show an increase both in mid-century and end-century compared to the historical period. In the mid-century, there is a difference in the magnitude of the rainfall increases with the SSP2-4.5 scenario projecting higher percentage changes compared to the other two scenarios. Across the scenarios between mid-century and end century, the SSP5-8.5 scenario projects higher percentage increases in JJA rainfall compared to other two scenarios.

Table 8.5: Projected changes in seasonal mean rainfall (percent change) - JJA

JJA	Mid-Century (%)		End-Century (%)	
	Mean	Range	Mean	Range
SSP1-2.6	3.3	0.8 to 9.6	5.0	0.8 to 10.7
SSP2-4.5	5.3	3.1 to 10.2	5.1	-3.7 to 14.6
SSP5-8.5	2.7	-1.3 to 9.4	7.4	-1.7 to 13.4

For the SON season, the rainfall is projected to increase both in mid-century and end century compared to the historical with higher percentage changes in the end century. When moving across scenarios, at the end of the century there are higher percentage changes in the rainfall when moving from SSP2-4.5 to SSP5-8.5 scenario.

Table 8.6: Projected changes in seasonal mean rainfall (percent change) - SON

SON	Mid-Century (%)		End-Century (%)	
	Mean	Range	Mean	Range
SSP1-2.6	4.1	0.0 to 7.1	4.9	1.7 to 8.0
SSP2-4.5	5.5	-0.7 to 12.8	8.0	3.3 to 13.8
SSP5-8.5	5.4	0.8 to 11.5	12.7	5.1 to 19.0

Figure. 8.3 shows the percentage changes in the seasonal mean rainfall (ensemble mean) over SEA regions in the end century relative to the historical period under the SSP5-8.5 scenario. As seen in Figure 8.3, the seasonal mean rainfall changes vary with seasons over land and ocean regions. Increases in rainfall can be seen over parts of Indochina across the four seasons.

For the DJF season, there are large percentage increases (>90%) over the climatologically dry regions of Thailand and Cambodia (see Figure 7.4). In their analysis of changes of CORDEX RCMs over the end-century (2070-2099) relative to the historical (1976-2005), Tangang et al. (2020) noted increased rainfall of 10-20% over Indochina, which was consistent with the changes from GCMs.

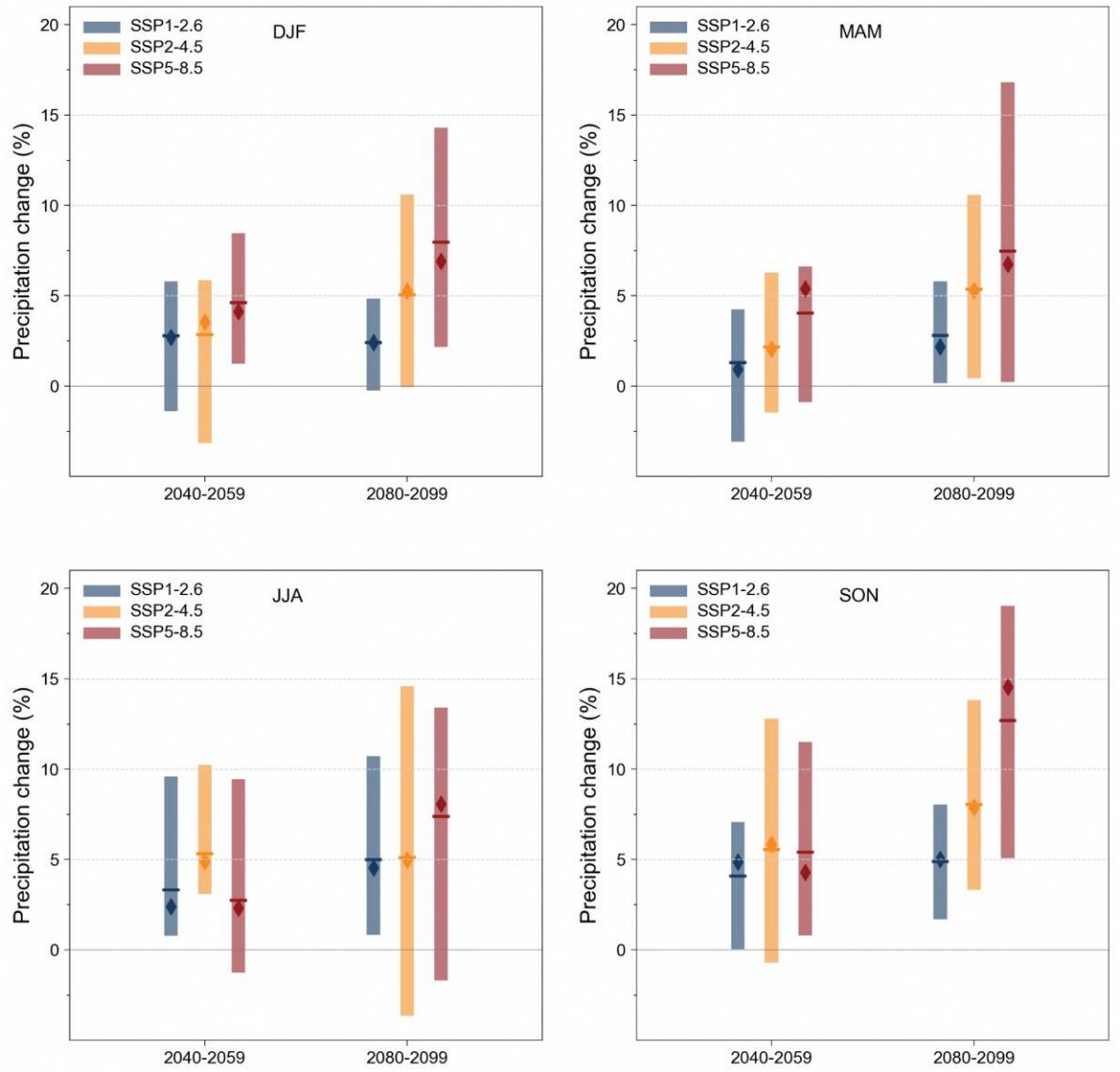

Figure 8.2: Percentage change of seasonal mean rainfall (pr) over the mid- (2040-59) and end-century (2080-99) period for the 6 downscaled GCMs (8km) over the SEA land relative to the historical (1995-2014) baselines. The line and diamond represent the mean and median using the 6 models, respectively.

During the MAM season, the seasonal mean rainfall is projected to increase (10-70%) over many SEA land regions. During the JJA season, the mean rainfall projections show increases (10-90%) over parts of Myanmar, Thailand, Malaysia, and around Java. Note that Java climatologically experiences little rainfall in JJA (see Figure 7.5) There is a percentage decrease (10-30%) in the mean rainfall over parts of Cambodia, Vietnam, Borneo, and New Guinea. For the SON season, the mean rainfall projections show percentage increases (10-90%) over the SEA nations with higher increases over Myanmar and around Nusa Tenggara. Tangang et al (2020) emphasize rainfall reduction of 10-30% in JJA, especially over Kalimantan and Sumatra and note that this drying has also been found in GCM simulations. They suggest it is linked to the equatorward contraction of the rising branch of the Hadley Circulation, the “deep tropical squeeze” discussed in Fu 2015. They also remark upon a reduction of 10-20% in mean rainfall over Cambodia, Vietnam, and eastern Thailand in the RCMs, which is not seen in the GCMs. These drying features are reflected in SINGV-MMM to some extent.

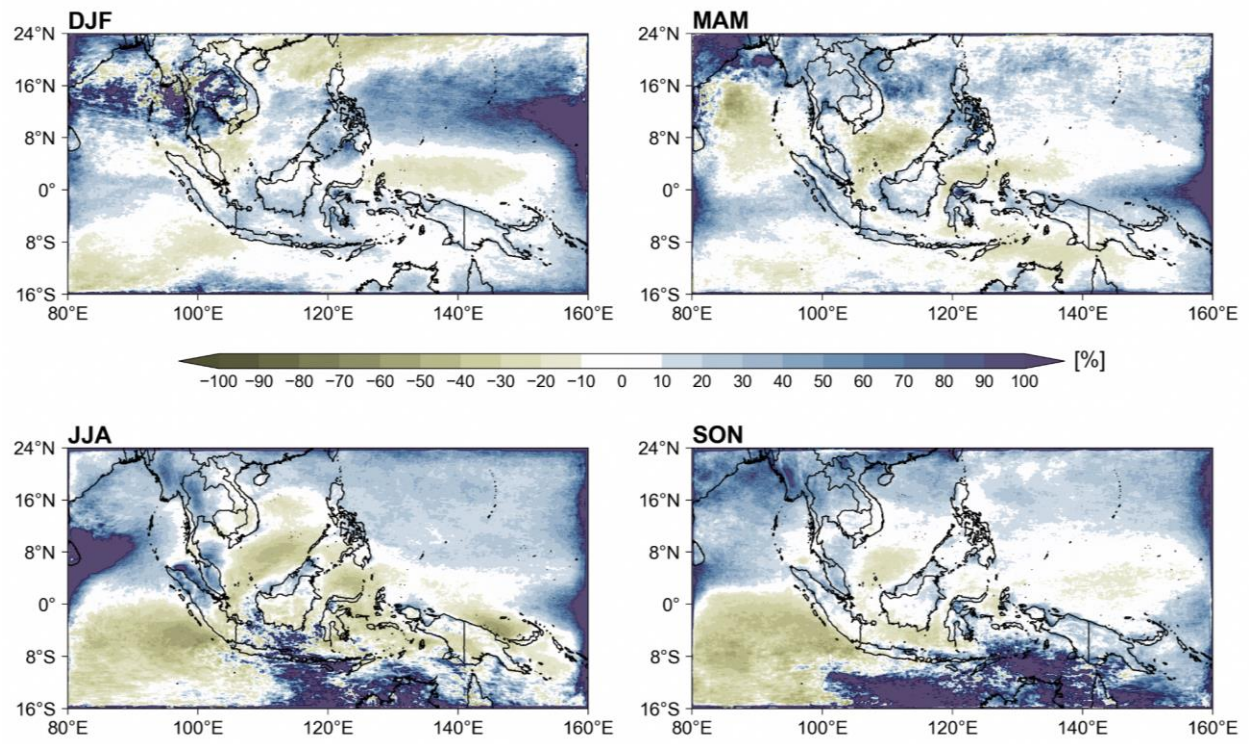

Figure 8.3: Percentage change of ensemble-mean downscaled (8km) changes in seasonal mean rainfall over end-century (2080-99) relative to the historical period (1995-2014) over the SEA domain under the SSP5-8.5 scenario.

8.3.3 Changes in rainfall extremes

Figure.8.4 shows the percentage changes in the maximum 1-day rainfall (RX1day) over SEA across different seasons in the end century relative to the historical under the SSP5-8.5 scenario. End-century RX1day is expected to increase in most of the SEA land regions across the four seasons.

During the DJF season, the projected RX1day percentage increases are largest over Thailand, Laos, and Cambodia. For the MAM season, the RX1day projections show increases (30%-70%) over the SEA land regions. During the JJA season, the projected RX1day increases (10%-100%) over most of the SEA land regions with decreases (-5% to -40%) around the Java sea. For the SON season, the RX1day projections increase (30%-100%) across the SEA land regions. Some of the largest percentage increases occur over climatologically dry regions (e.g. Indochina in DJF, around the Java sea in JJA).

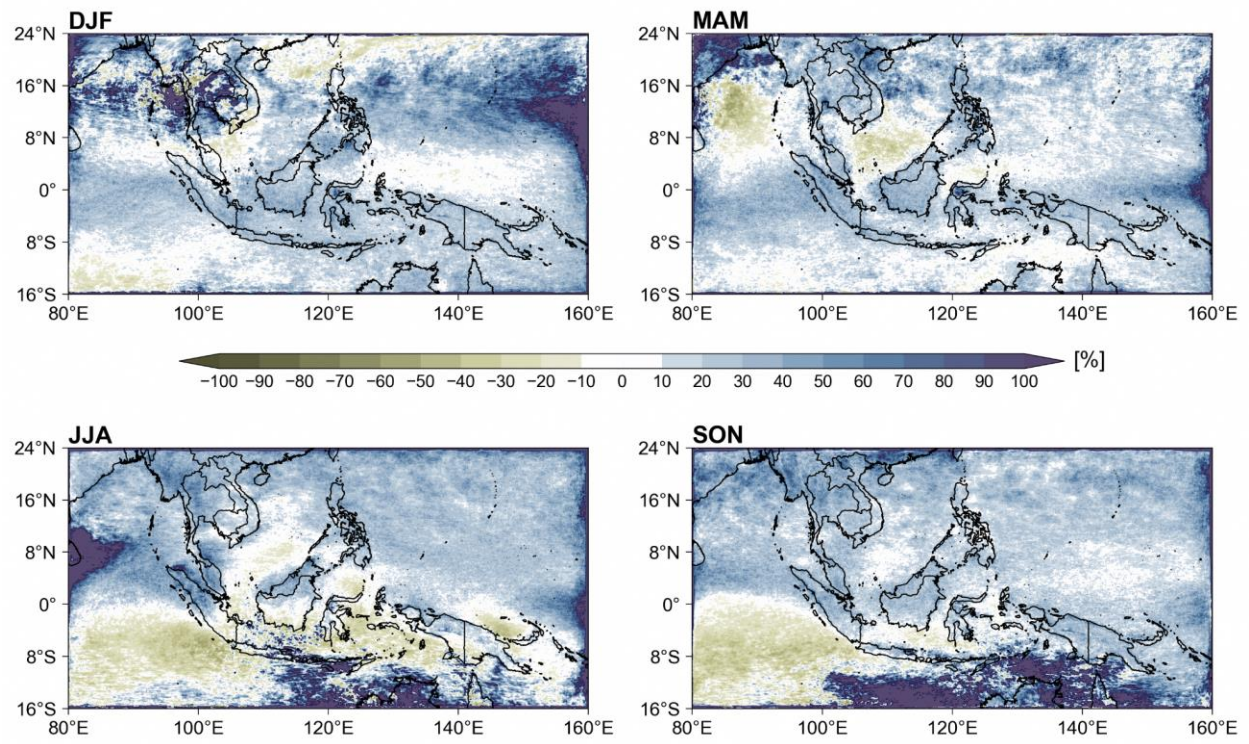

Figure 8.4: Percentage change of ensemble-mean downscaled (8km) changes in seasonal RX1day over end-century (2080-99) relative to the historical period (1995-2014) over the SEA domain under the SSP5-8.5 scenario.

Figure 8.5 shows the percentage changes in the maximum 5-day rainfall (RX5day) over SEA across different seasons in the end century relative to the historical under the high emission scenario (SSP5-8.5). RX5day is projected to increase with warming over much of SEA in most of the seasons, with features qualitatively similar to RX1day. During the DJF season, the RX5day projections show an increase (10%-100%) over much of the domain, with higher percentage increases over Thailand, Laos, and Cambodia. For the MAM season, the projected RX5day increases (30%-70%) across much of SEA land in the end century with some of the largest increases occurring west of Myanmar. During the JJA season, the projected RX5day increases with higher percentages (50%-90%) over the northern SEA nations. For the SON season, the RX5day projections show an increase (30%-100%) over most of the SEA nations.

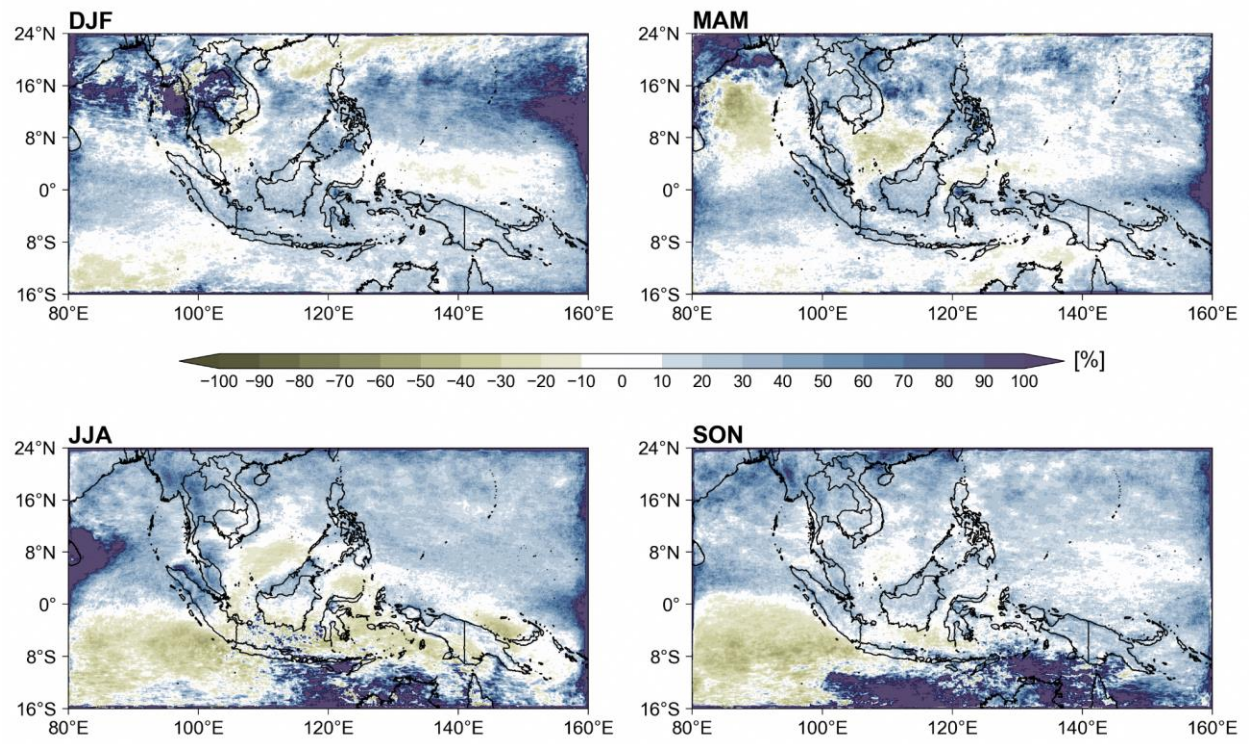

Figure 8.5: Percentage change of ensemble-mean downscaled (8km) changes in seasonal RX5day over end-century (2080-99) relative to the historical period (1995-2014) over the SEA domain under the SSP5-8.5 scenario.

8.3.4 Changes in annual mean temperature

Figure. 8.6 shows the projected changes in the annual mean near-surface air temperatures (tas) over SEA and SEA land regions during the mid-century (2040-59) and end century (2080-99) compared to historical (1995-2014) under three SSP scenarios using 8 km downscaled simulations. For readability, they are also shown in tabular form in Tables 8.7-8.8. Annual mean near-surface air temperatures increase over SEA and SEA land regions under different SSP scenarios. Over the SEA domain, the multi-model mean projected temperatures are expected to increase by at least 0.8ºC in the mid-century and by at least 1.0 ºC in the end century. Based on the multi-model mean projections, SEA land will experience increased warming as compared to the SEA domain by 0.1 ºC to 0.7 ºC (Tables 8.7 and 8.8) and up to 4.0 ºC by the end of the century. Land-amplified warming has been observed across multiple climate models, and can be explained by a simple analytical theory (Bryne and O'Gorman 2018)

Table 8.7: Projected changes in annual mean temperature - SEA

ANN	Mid-Century (ºC)		End-Century (ºC)	
	Mean	Range	Mean	Range
SSP1-2.6	0.8	0.6 to 1.1	1.0	0.5 to 1.4
SSP2-4.5	1.1	0.7 to 1.5	1.7	1.2 to 2.5
SSP5-8.5	1.4	0.9 to 1.9	3.3	2.4 to 4.4

Table 8.8: Projected changes in annual mean temperature - SEA land

ANN	Mid-Century (ºC)		End-Century (ºC)	
	Mean	Range	Mean	Range
SSP1-2.6	1.0	0.6 to 1.4	1.1	0.5 to 1.7
SSP2-4.5	1.2	0.8 to 1.8	2.1	1.4 to 3.0
SSP5-8.5	1.6	1.1 to 2.2	4.0	2.9 to 5.4

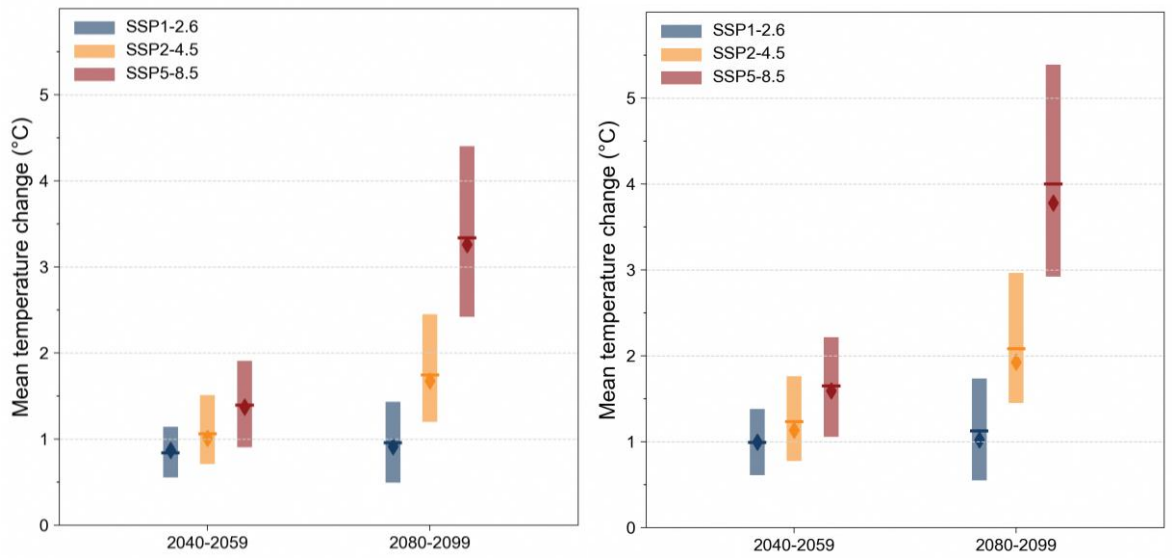

Figure 8.6: Average changes in annual mean near-surface air temperature (tas) over the mid- (2040-59) and end-century (2080-99) period for the 6 downscaled GCMs (8km) over the SEA domain (left) and SEA land only (right) relative to the historical (1995-2014) baselines. The line and diamond represent the mean and median using the 6 models, respectively.

Figure.8.7 shows the projected changes in the annual maximum (tasmax) and minimum near-surface air temperatures (tasmin) over SEA land regions in the mid-century and end century compared to historical under three SSP scenarios using 8 km downscaled GCM simulations. For readability, they are also shown in tabular form in Tables 8.9-8.10. As seen in Figure .8.7, the tasmax and tasmin temperatures over SEA land increase by similar amounts with warming across the different scenarios and time periods. There is a minimum increase of 1^{o}C of the tasmax and tasmin in mid and end century. Across the scenarios, towards the end century there is a higher degree of increases in tasmax and tasmin over SEA land regions under the SSP5-8.5 scenario. The qualitative changes in tasmax and tasmin are similar to those in tas (Figure 8.6).

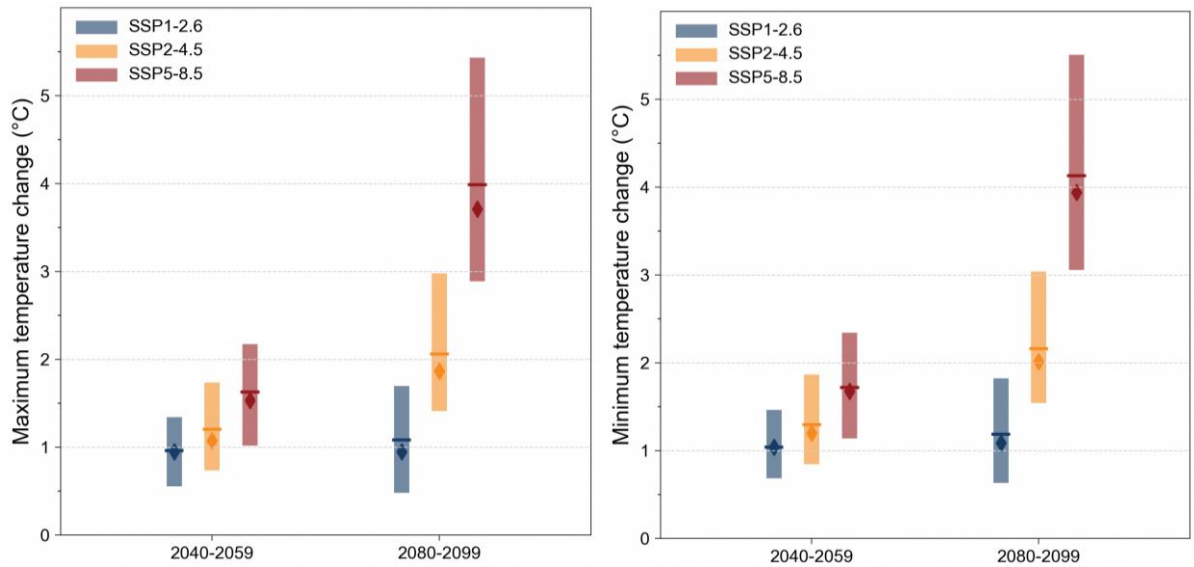

Figure 8.7: Average changes in annual maximum (tasmax) and minimum (tasmin) near-surface air temperature over the mid- (2040-59) and end-century (2080-99) period for the 6 downscaled GCMs (8km) over the SEA land relative to the historical (1995-2014) baselines. The line and diamond represent the mean and median using the 6 models, respectively.

Table 8.9: Projected changes in annual maximum temperature - SEA land

ANN	Mid-Century (ºC)		End-Century (ºC)	
	Mean	Range	Mean	Range
SSP1-2.6	1.0	0.6 to 1.3	1.1	0.5 to 1.7
SSP2-4.5	1.2	0.7 to 1.7	2.1	1.4 to 3.0
SSP5-8.5	1.6	1.0 to 2.2	4.0	2.9 to 5.4

Table 8.10: Projected changes in annual minimum temperature - SEA land

ANN	Mid-Century (ºC)		End-Century (ºC)	
	Mean	Range	Mean	Range
SSP1-2.6	1.0	0.7 to 1.5	1.2	0.6 to 1.8
SSP2-4.5	1.3	0.8 to 1.9	2.2	1.5 to 3.0
SSP5-8.5	1.7	1.1 to 2.3	4.1	3.1 to 5.5

8.3.5 Changes in seasonal mean temperature

Figure 8.8 shows the projected changes in the seasonal mean of daily maximum near surface temperatures (tasmax) over SEA land regions in the mid-century and end century relative to the historical under three SSP scenarios. For readability, they are also shown in tabular form in Tables 8.11-8.14. The projected tasmax temperatures increase with warming over SEA land regions across all the seasons. Across all seasons, the projected multi-model tasmax increases with warming in mid-century and end century. Across the scenarios, towards the end of the century there is an increased mean seasonal maximum temperature with higher increases under the SSP5-8.5 scenario (~3.9ºC). Based on the multi-model mean, across the seasons, mid-century tasmax would change from 0.9 ºC -1.7 ºC while end-century seasonal tasmax would change from 1.0 ºC -4.1 ºC.

Table 8.11: Projected changes in seasonal maximum temperature - DJF

DJF	Mid-Century (ºC)		End-Century (ºC)	
	Mean	Range	Mean	Range
SSP1-2.6	0.9	0.6 to 1.3	1.1	0.5 to 1.6
SSP2-4.5	1.2	0.6 to 1.6	2.0	1.2 to 2.8
SSP5-8.5	1.6	0.9 to 2.1	3.9	2.8 to 5.1

Table 8.12: Projected changes in seasonal maximum temperature - MAM

MAM	Mid-Century (ºC)		End-Century (ºC)	
	Mean	Range	Mean	Range
SSP1-2.6	1.1	0.6 to 1.4	1.2	0.5 to 1.9
SSP2-4.5	1.2	0.8 to 1.9	2.2	1.5 to 3.2
SSP5-8.5	1.7	1.0 to 2.2	4.1	2.9 to 5.7

Table 8.13: Projected changes in seasonal maximum temperature - JJA

JJA	Mid-Century (ºC)		End-Century (ºC)	
	Mean	Range	Mean	Range
SSP1-2.6	0.9	0.5 to 1.5	1.0	0.4 to 1.8
SSP2-4.5	1.2	0.8 to 1.9	2.1	1.3 to 3.2
SSP5-8.5	1.6	1.0 to 2.4	4.0	2.9 to 5.7

Table 8.14: Projected changes in seasonal maximum temperature - SON

SON	Mid-Century (ºC)		End-Century (ºC)	
	Mean	Range	Mean	Range
SSP1-2.6	0.9	0.5 to 1.2	1.0	0.4 to 1.6
SSP2-4.5	1.1	0.8 to 1.7	2.0	1.5 to 2.7
SSP5-8.5	1.6	1.2 to 2.1	3.9	2.8 to 5.3

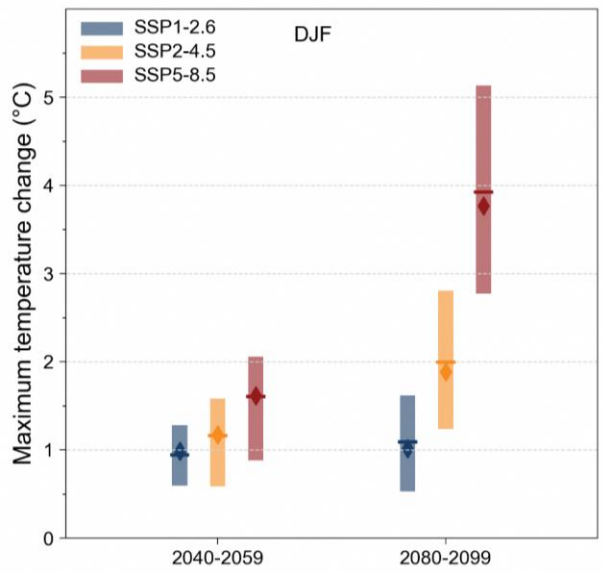

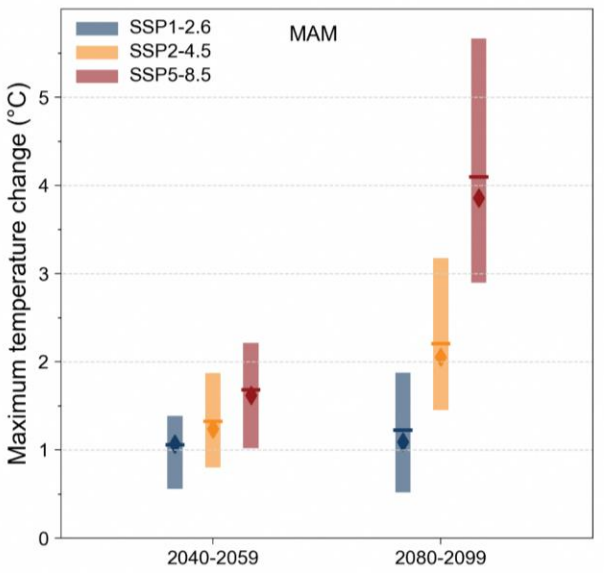

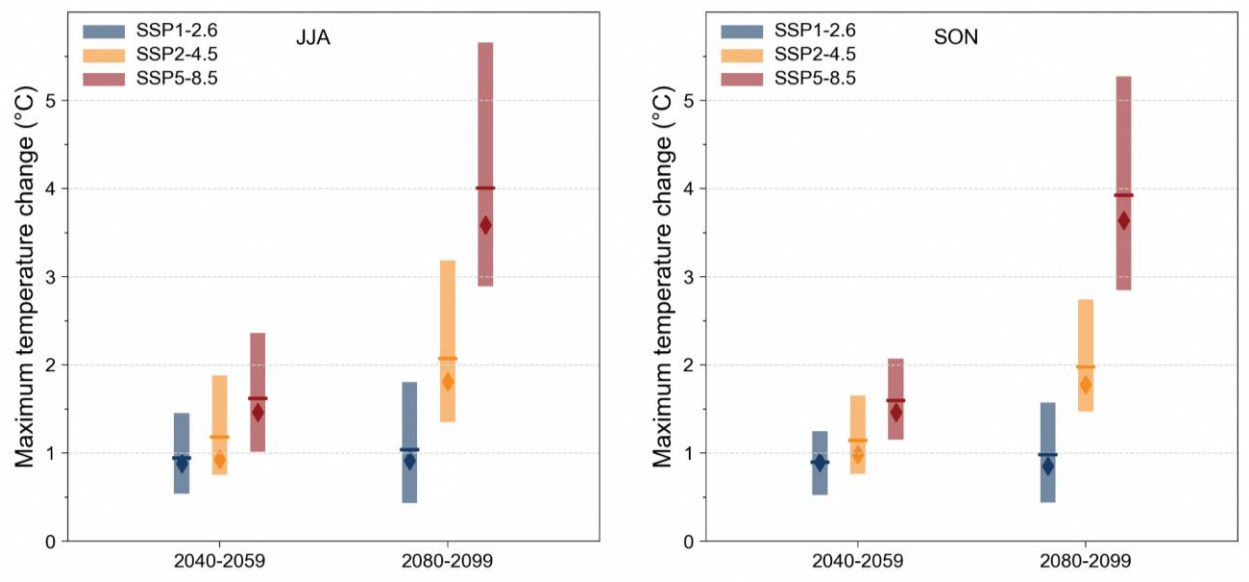

Figure 8.8: Average changes in seasonal maximum near-surface air temperature (tasmax) over the mid- (2040-59) and end-century (2080-99) period for the 6 downscaled GCMs (8km) over the SEA land relative to the historical (1995-2014) baselines. The line and diamond represent the mean and median using the 6 models, respectively.

Figure 8.9 shows the projected changes in the seasonal mean near-surface air temperatures over SEA in the end century (2080-99) relative to the historical (1995-2014) under the SSP5-8.5 scenario. The near-surface air temperatures are projected to increase in the end century over the SEA domain with higher increases over the land compared to the surrounding oceanic regions. During the DJF season, the projections of near-surface air temperatures increase in the range of 2.5 to 5.5^{o}C in the end century with higher values over Myanmar, Thailand, Laos and Cambodia. For the MAM season, the projected near-surface air temperatures increase by 2.5 to 6.0^{o}C in the end century with higher increases over Myanmar, Thailand and Laos. During the JJA season, the projected near-surface air temperatures increased in the range of 2.0 to 6.0^{o}C with higher increases over Laos, Vietnam, and Indonesia. The changes in JJA are of comparable magnitude to changes in JJA end-century (2070-2099) versus historical (1980-2009) temperatures in V2 (Chapter 5). For the SON season, the projections of near-surface air temperatures show increases by 2.0 to 5.0^{o}C in the end century.

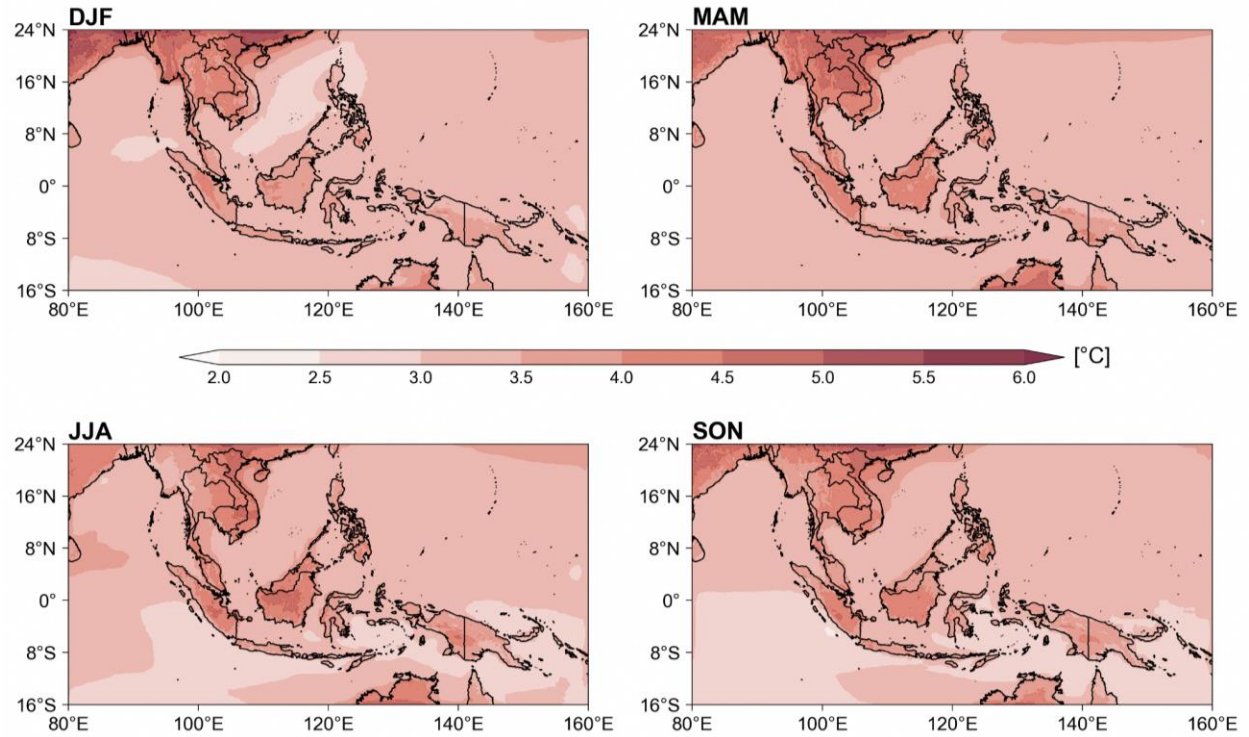

Figure 8.9: Ensemble-mean (6 downscaled GCMs 8 km) changes in seasonal mean near-surface air temperature over end-century (2080-99) relative to the historical period (1995-2014) over the SEA domain under the SSP5-8.5 scenario.

8.3.6 Changes in temperature extremes

Figure 8.10 shows the projected changes in the seasonal maximum of daily maximum temperatures (TXx) over the SEA domain in the end century relative to the historical under the SSP5-8.5 scenario. As seen in the Figure 8.10, the projected TXx increases over the SEA in the end century across the seasons with higher increases over the land regions compared to oceans. During the DJF season, the projected TXx increases in the range of 2.5 to 6.0ºC. For the MAM season, the projections of TXx show increases by 3.0 to 6.0ºC with higher increases over Laos, Vietnam, Borneo, Indonesia, and New Guinea. During the JJA season, the projected TXx increases in the range of 3.0 to 6.5ºC with higher increases over Thailand, Cambodia, Laos, Vietnam, Borneo, and Indonesia. For the SON season, the projected TXx increases by 3.0 to 6.0ºC with higher increases over Cambodia, Laos, Vietnam, Borneo, and Indonesia.

Figure 8.11 shows the projected changes in the seasonal minimum of daily minimum temperatures (TNn) over the SEA in the end century relative to the historical under the SSP5-8.5 scenario. Projected TNn increases over the SEA with higher increases over the land regions. During the DJF season, the projected TNn increases in the range of 3.0 to 6.0ºC with higher increases over Myanmar, Thailand, and Cambodia. For the MAM season, the projected TNn increases by 3.0 to 6.5ºC with higher increases over Myanmar, Thailand, and Cambodia. During the JJA season, the projected TNn increases in the range of 3.0 to 5.0ºC. For the SON season, the projected TNn increases in the range of 3.0 to 6.0ºC with higher increases over Myanmar, Thailand, and Cambodia.

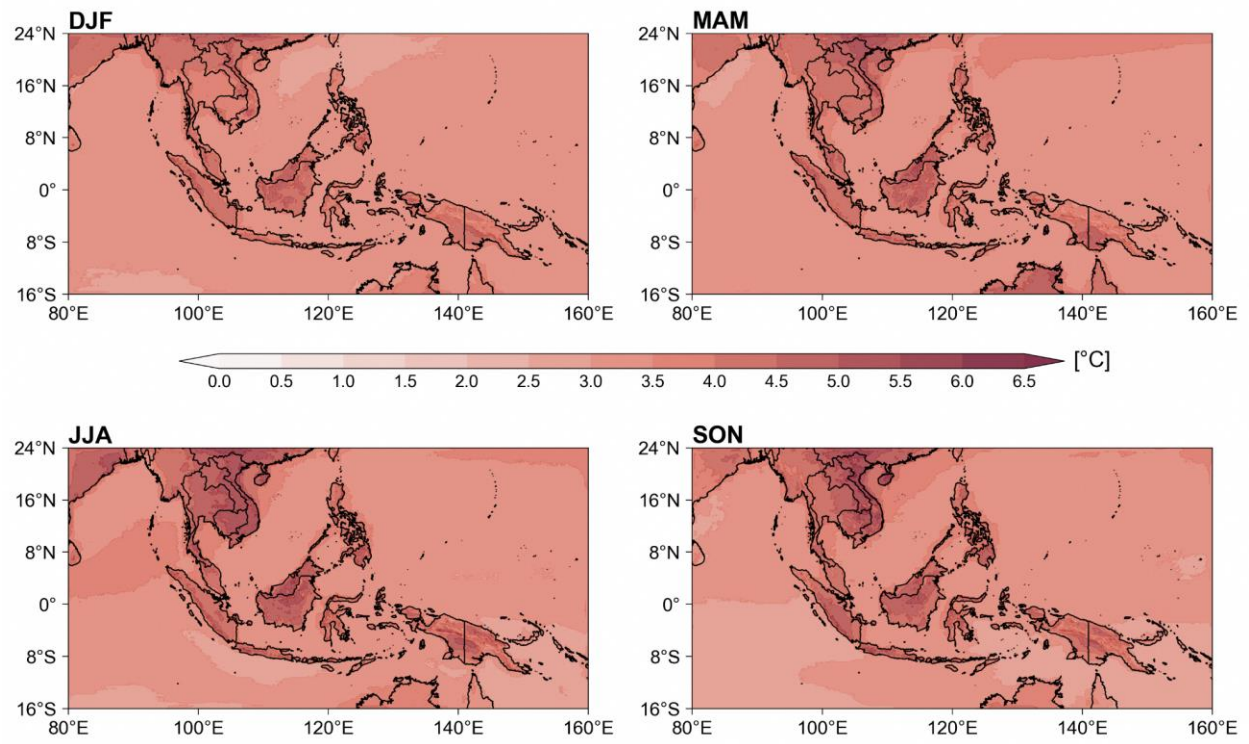

Figure 8.10: Ensemble-mean (6 downscaled GCMs 8 km) changes in seasonal maximum of daily maximum temperature (TXx) over end-century (2080-99) relative to the historical period (1995-2014) over the SEA domain under the SSP5-8.5 scenario.

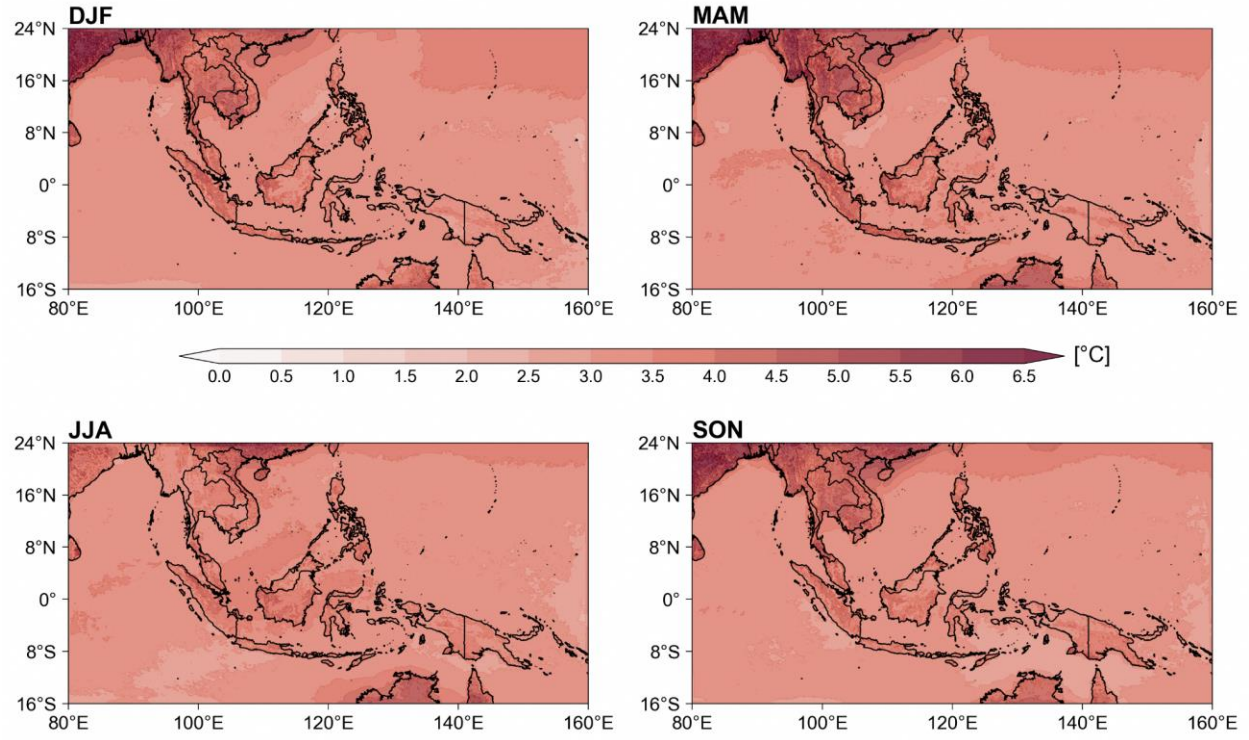

Figure 8.11: Ensemble-mean (6 downscaled GCMs 8 km) changes in seasonal minimum of daily minimum temperature (TNn) over end-century (2080-99) relative to the historical period (1995-2014) over the SEA domain under the SSP5-8.5 scenario.

8.3.7 Changes in relative humidity

Figure 8.12 shows the percentage changes in the annual mean near-surface relative humidity (hurs) over SEA and SEA land regions in the mid-century and end century relative to the historical under three SSP scenarios. For readability, they are also shown in tabular form in Tables 8.15-8.16. As seen in Figure 8.12, the multi-model mean indicates hurs increases over SEA and decreases over SEA land across scenarios and time periods. Similar to the warming over land, decreases in land hurs with warming have been reported in other studies and has some theoretical support (Byrne and O'Gorman 2018).

Table 8.15: Projected changes in annual mean near-surface relative humidity - SEA

ANN	Mid-Century (%)		End-Century (%)	
	Mean	Range	Mean	Range
SSP1-2.6	0.13	-0.05 to 0.27	0.10	-0.15 to 0.27
SSP2-4.5	0.22	0.03 to 0.41	0.29	0.07 to 0.53
SSP5-8.5	0.27	0.12 to 0.42	0.38	-0.09 to 0.83

Table 8.16: Projected changes in annual mean near-surface relative humidity - SEA land

ANN	Mid-Century (%)		End-Century (%)	
	Mean	Range	Mean	Range
SSP1-2.6	-0.20	-0.65 to 0.23	-0.21	-0.73 to 0.29
SSP2-4.5	-0.18	-0.84 to 0.21	-0.57	-1.20 to -0.07
SSP5-8.5	-0.32	-1.08 to 0.11	-1.35	-2.73 to -0.38

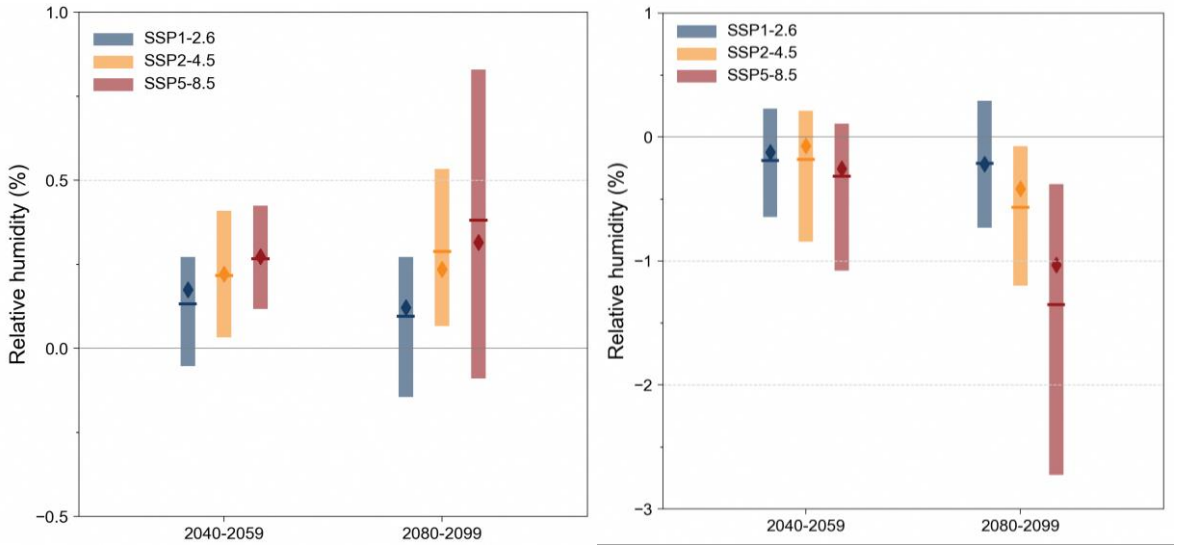

Figure 8.12: Average changes in annual mean near-surface relative humidity (hurs) over the mid- (2040-59) and end-century (2080-99) period for the 6 downscaled GCMs (8km) over the SEA domain (left) and SEA land only (right), with respect to their historical (1995-2014) baselines. The line and diamond represent the mean and median using the 6 models, respectively.

Figure 8.13 shows the percentage changes of seasonal mean hurs over SEA and SEA land regions in the mid-century and end century relative to the historical under three SSP scenarios. There are seasonal differences in the projected hurs over SEA and SEA land regions in mid-century and end century. In general, percentage changes in multi-model mean hurs over SEA land are either small or negative, ranging from 0 to -1.9%. For readability, they are also shown in tabular form in Tables 8.17-8.20.

During the DJF season, in the mid-century the projected multi-model mean hurs remained unchanged in all three scenarios. In the end century, the projected multi-model mean hurs decreased by 0.0 to -0.9%.

Table 8.17: Projected changes in seasonal mean near-surface relative humidity

DJF	Mid-Century (%)		End-Century (%)	
	Mean	Range	Mean	Range
SSP1-2.6	0.0	-0.4 to 0.6	0.0	-0.4 to 0.4
SSP2-4.5	0.0	-0.4 to 0.6	-0.3	-0.5 to 0.1
SSP5-8.5	0.0	-0.9 to 0.7	-0.9	-1.8 to -0.3

For the MAM season, in the mid-century the projected multi-model mean hurs decreases in the range of -0.4 % to -0.5%. In the end century, the

projected multi-model mean hurs decreases by -0.6% to -1.3%.

Table 8.18: Projected changes in seasonal mean near-surface relative humidity

MAM	Mid-Century (%)		End-Century (%)	
	Mean	Range	Mean	Range
SSP1-2.6	-0.4	-0.9 to 0.2	-0.6	-1.3 to 0.3
SSP2-4.5	-0.4	-1.2 to 0.1	-0.8	-1.6 to 0.2
SSP5-8.5	-0.5	-1.1 to 0.0	-1.3	-2.7 to -0.4

During the JJA season, in the mid-century the projected hurs decreases in the range of -0.2% to -0.6%. In the end century, the projected hurs decreases by -0.2% to -1.9%.

Table 8.19: Projected changes in seasonal mean near-surface relative humidity

JJA	Mid-Century (%)		End-Century (%)	
	Mean	Range	Mean	Range
SSP1-2.6	-0.2	-1.0 to 0.2	-0.2	-0.6 to 0.2
SSP2-4.5	-0.2	-1.1 to 0.3	-0.8	-1.9 to -0.1
SSP5-8.5	-0.6	-1.5 to 0.0	-1.9	-3.7 to -0.7

For the SON season, in the mid-century the projected hurs decreases in the range of -0.1 % to -0.2%. In the end century, the projected hurs changes range from 0% to -1.3%.

Table 8.20: Projected changes in seasonal mean near-surface relative humidity

SON	Mid-Century (%)		End-Century (%)	
	Mean	Range	Mean	Range
SSP1-2.6	-0.1	-0.9 to 0.5	0.0	-0.6 to 0.4
SSP2-4.5	-0.1	-0.9 to 0.6	-0.4	-1.3 to 0.2
SSP5-8.5	-0.2	-0.9 to 0.6	-1.3	-3.0 to 0.1

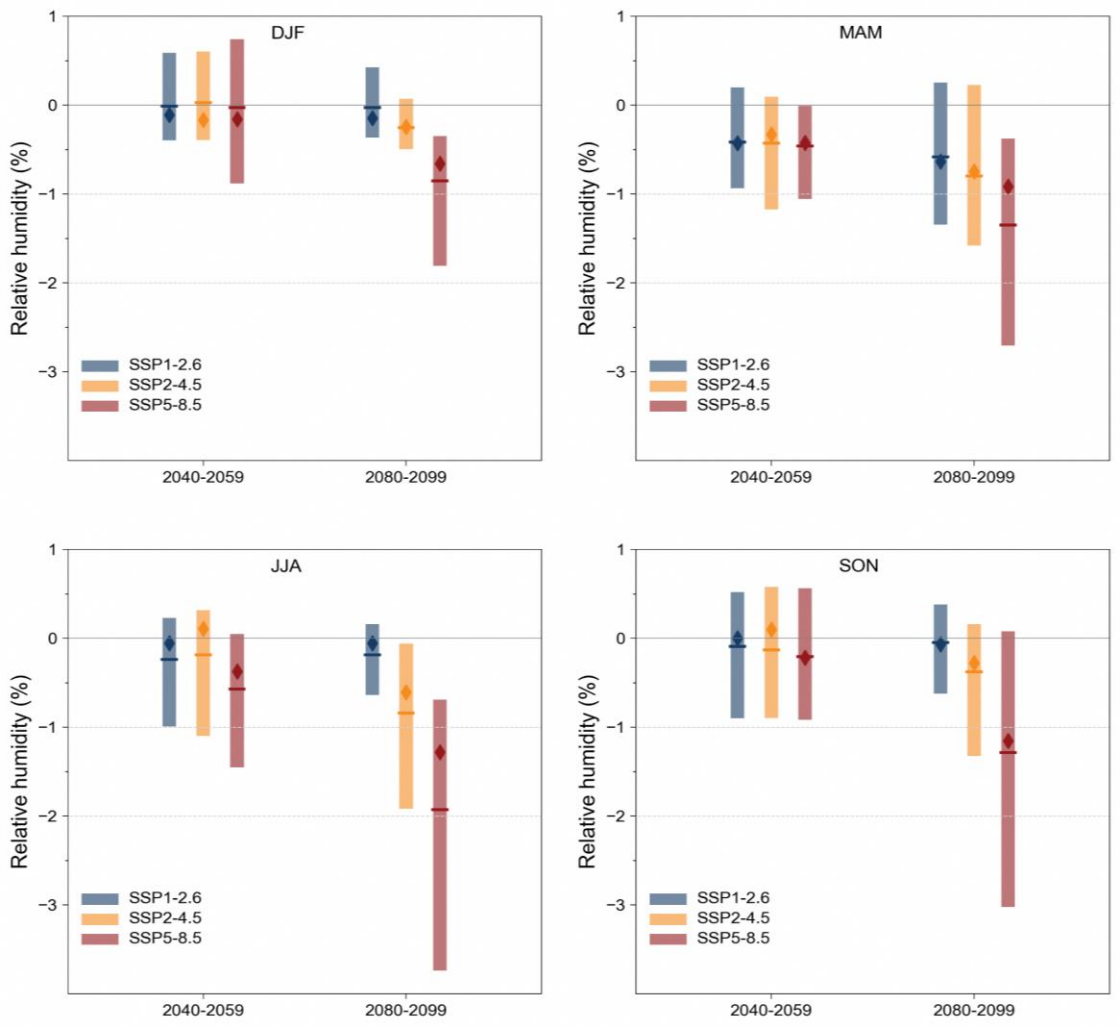

Figure 8.13: Average changes in seasonal mean near-surface relative humidity (hurs) over the mid- (2040-59) and end-century (2080-99) period for the 6 downscaled GCMs (8km) over the SEA land relative to the historical (1995-2014) baselines. The line and diamond represent the mean and median using the 6 models, respectively.

Figure 8.14 shows the multi-model mean percentage changes in the seasonal mean hurs over the SEA in the end century relative to the historical under the SSP5-8.5 scenario. As seen in Figure 8.14, there are seasonal differences in the hurs over the SEA land and ocean regions. During the DJF season, the projected hurs decreases (-1% to -6%) over most of the SEA land regions and increases (1% to 4%) over oceans in the end century.

For the MAM season, the projected hurs decreases in the range of -1% to -6% over the SEA land regions and slightly increases (1% to 3%) over the oceans.

During the JJA season, the projected hurs decreases (-1% to -9%) over the land regions with higher decreases over Cambodia, Vietnam, Indonesia, and New Guinea. The projected hurs over the oceanic regions increases (1% to 4%) during the JJA season. For the SON season, the projected hurs decreases (-1% to -7%) over the land regions and increases (1% to 6%) over the oceans.

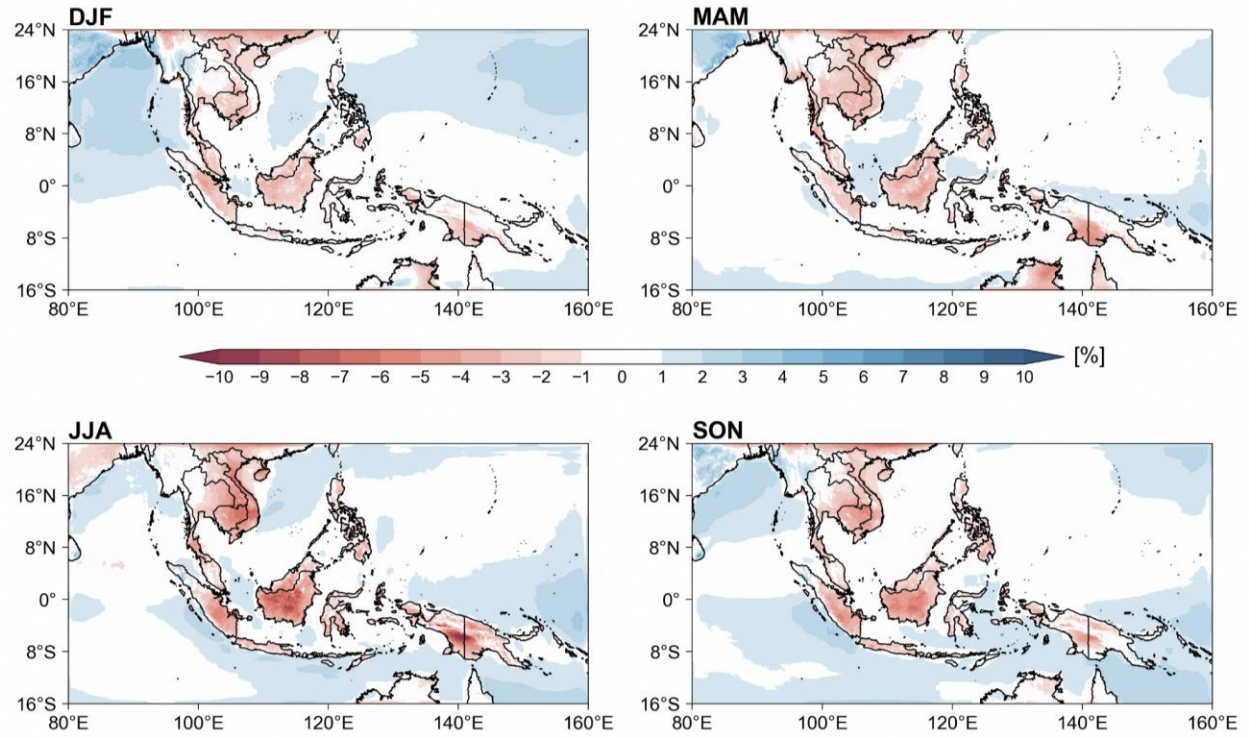

Figure 8.14: Ensemble-mean downscaled (8km) changes in seasonal mean near-surface relative humidity over end-century (2080-99) relative to the historical period (1995-2014) over the SEA domain under the SSP5-8.5 scenario.

8.4 Changes in Regional Climate Drivers

In this section we present projected changes in the important regional climate drivers discussed in Chapters 3, 4, 5, and 7. While we don't expect significant changes in the projected regional climate drivers in the downscaled simulations as compared to that seen from the driving GCMs, it is worth investigating if there are any notable differences.

8.4.1 Monsoons

In DJF (see Figure 8.15a), changes in wind speeds are small over the South China Sea, where some of the strongest climatological winds occur. There are anomalous westerlies east of the Philippines as well as anomalous easterlies west of Sumatra, representing a weakening of the climatological flow. Similar westerly and easterly anomalies can be seen in Tangang et al 2020, which examined changes in end-century (2071-2099) winds under RCP8.5 using the CORDEX ensemble, with changes over the South China

Sea being within 1 m/s. These westerly and easterly anomalies are also similar to those in SON (Figure 8.15d). The changes in winds in MAM are generally small (Figure 8.15b).

In JJA, (Figure 8.15c) there is a strengthening of the monsoon flow over Indochina, with an anomalous easterly flow over much of the western Maritime Continent. Tangang et al 2020 found a similar westerly flow over Indochina and easterly flow over Sumatra towards the Indian ocean. In all seasons, a weakening of the flow with anomalous easterlies over the Indian ocean can be seen. Overall, the wind anomalies are most notable in JJA.

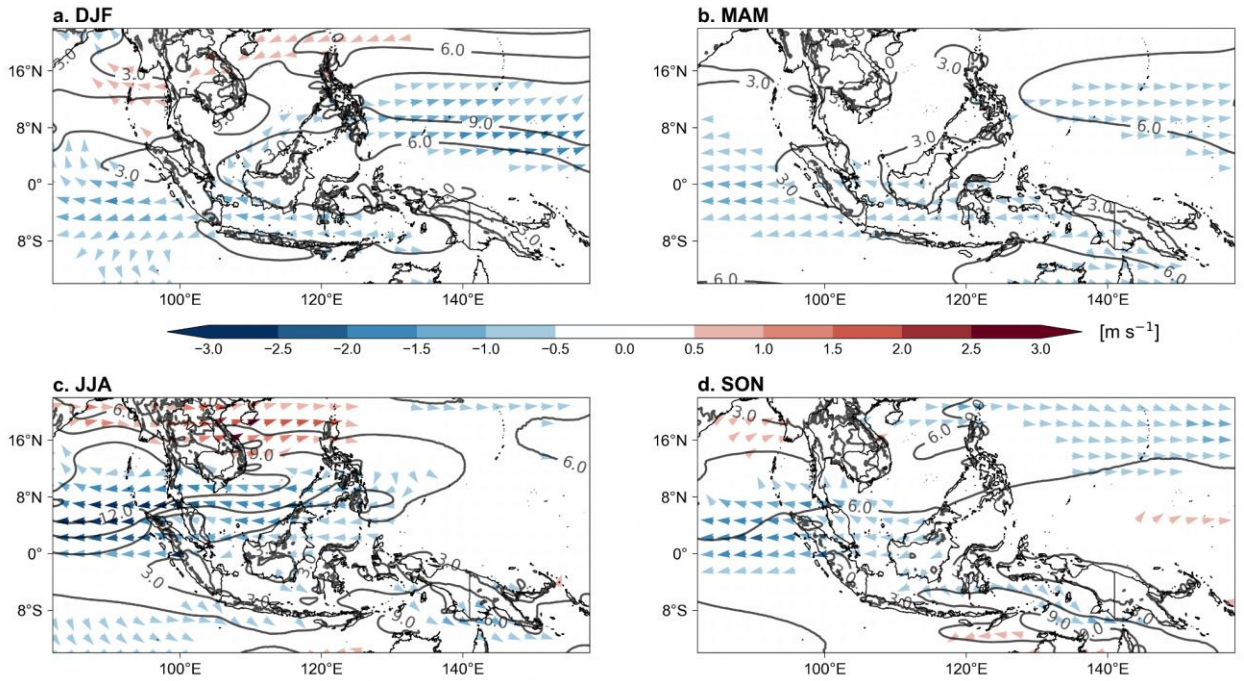

Figure 8.15: shows the change in 850 hPa wind direction (arrows, colors indicate magnitude) and climatological wind speeds (contours) over Southeast Asia during 2080-2099 in SSP5-8.5 with respect to 1995-2014 in SINGV-MMM (containing six 8km model outputs).

8.4.2 Northeast Monsoon surge

As highlighted in Section 4.5.5, monsoon cold surges are a key synoptic feature of the boreal winter circulation over the Maritime Continent and can lead to extreme rainfall. The cold surges can also be enhanced by the presence of a favorable phase of the MJO (e.g. Lim et al., 2017) and might also aid the MJO in its passage across the Maritime Continent (Pang et al., 2018). Given the importance of boreal winter monsoon cold surges to the weather and climate of SEA, it is important to analyse how the cold surges are projected to change under global warming in the V3 downscaled simulations. It is also important to check if there are any important differences in the downscaled projections of cold surges as compared to that seen in the driving CMIP6 GCMs (see Section 4.5.5 and Figure 4.10).

The changes over the Western Maritime Continent are relatively small (Figure 8.16). There is a weakening in surge winds over the Java Sea, and more rain over areas east of Borneo. There are also increased outflows towards Indochina. There are some similarities between changes in the composite over surge days (which occur in NDJF by definition) and the changes in wind speed over DJF - small changes over the South China Sea, anomalous westerlies east of the Philippines as well as anomalous easterlies west of Sumatra. The pattern of rainfall change is also similar to that of DJF rainfall e.g. increases over the Java sea and east of the Philippines.

Similar to the parent GCMs, the downscaled simulations predict easterly anomalies over Indochina and west of Sumatra, as well as westerly anomalies north of New Guinea. There is also an increase in multi-model surge frequency from 17% in historical to 18% in SSP5-8.5, similar to the parent GCMs, where surge frequency increases from 18% to 19%. In contrast, the magnitude of precipitation and rainfall changes in the downscaled simulations are also enhanced relative to the parent GCMs. There are also differences in the details of rainfall: the multimodel mean of the parent GCMs predicts rainfall increase over South Sumatra and Borneo, but the downscaled simulation places the rainfall increase primarily over the Java Sea.

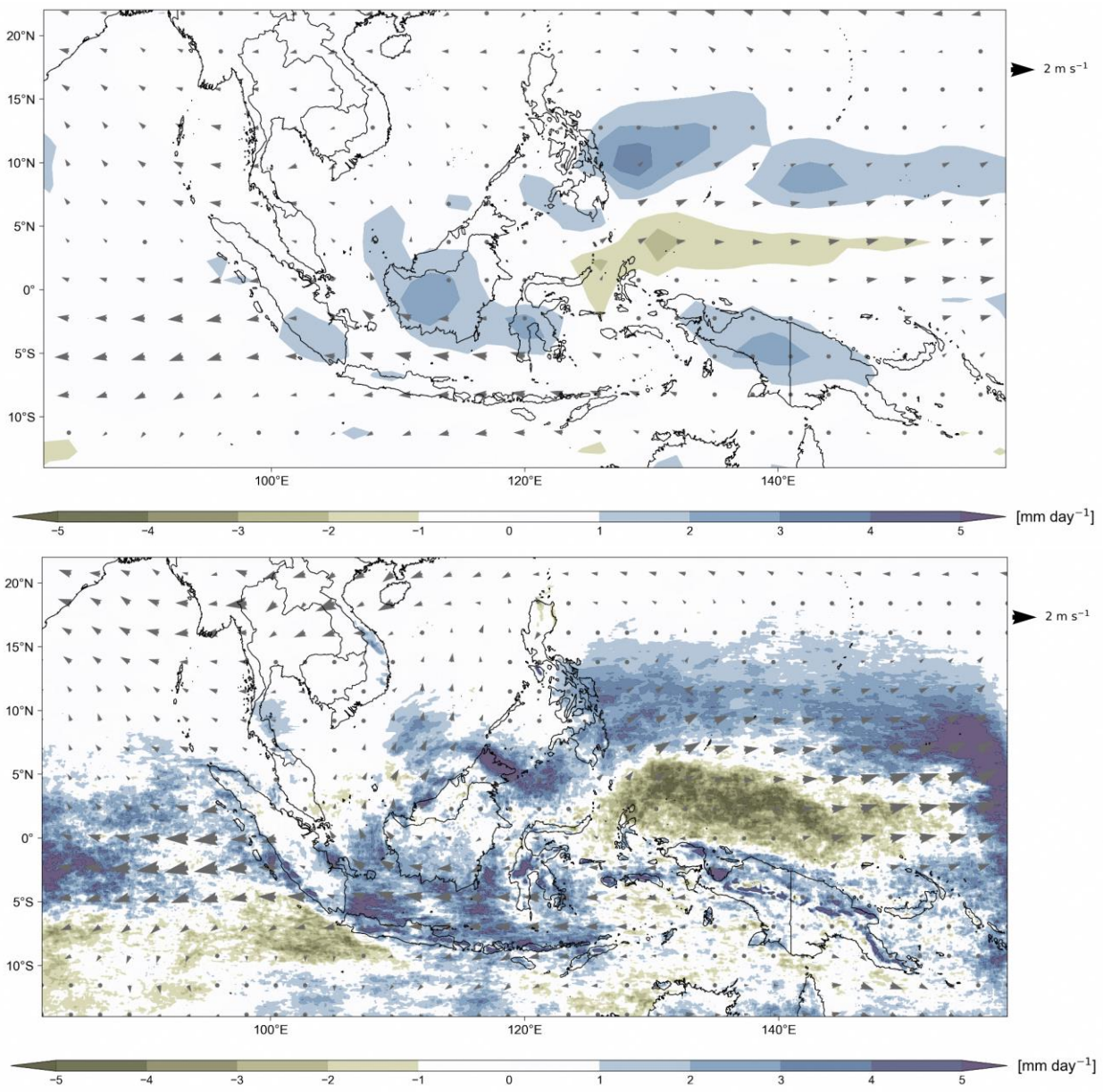

Figure 8.16: Upper panel shows the change in 850 hPa wind direction (arrows) and rainfall (shaded) composited over surge days from 2080-2099 in SSP5-8.5 with respect to 1995-2014 in 6 GCMs, regridded to 1.5 x1.5 (those used for downscaling). Lower panel shows the change in 850 hPa wind direction (arrows) and rainfall (shaded) composited over surge days from 2080-2099 in SSP5-8.5 with respect to 1995-2014 in SINGV-MMM (containing six 8km model outputs).

8.4.3 ENSO Teleconnection

Here in this section we focus on 6 SINGV-RCMs and their forcing GCMs to address changes in the ENSO teleconnection. Here we show that RCMs and GCMs produce very similar and consistent spatial patterns of the ENSO teleconnection (negative over the equatorial central MC and positive over the western Pacific) for both historical and future periods. The full results for the historical period are shown in chapter 7, section 7.5.3 Fig. 7.17. As to the future change (Figure 8.17), GCMs and RCMs both suggest that the negative correlation area over the equatorial MC is enlarged. The positive correlation area over the eastern MC and western Pacific are reduced, and the negative correlation extends to the east. These agree with the understanding that the whole zonal dipole pattern of the ENSO teleconnection shifts eastward, as shown by 32 GCMs in Chapter 4 and in our recent study (Chen et al. 2023).

Besides the large-scale consistency with GCMs, RCMs do offer additional detailed spatial representation of the ENSO teleconnection, especially over the mountainous islands (e.g. over New Guinea). Future studies may look into ENSO-induced rainfall variability at the local scale enabled by the high-resolution RCMs.

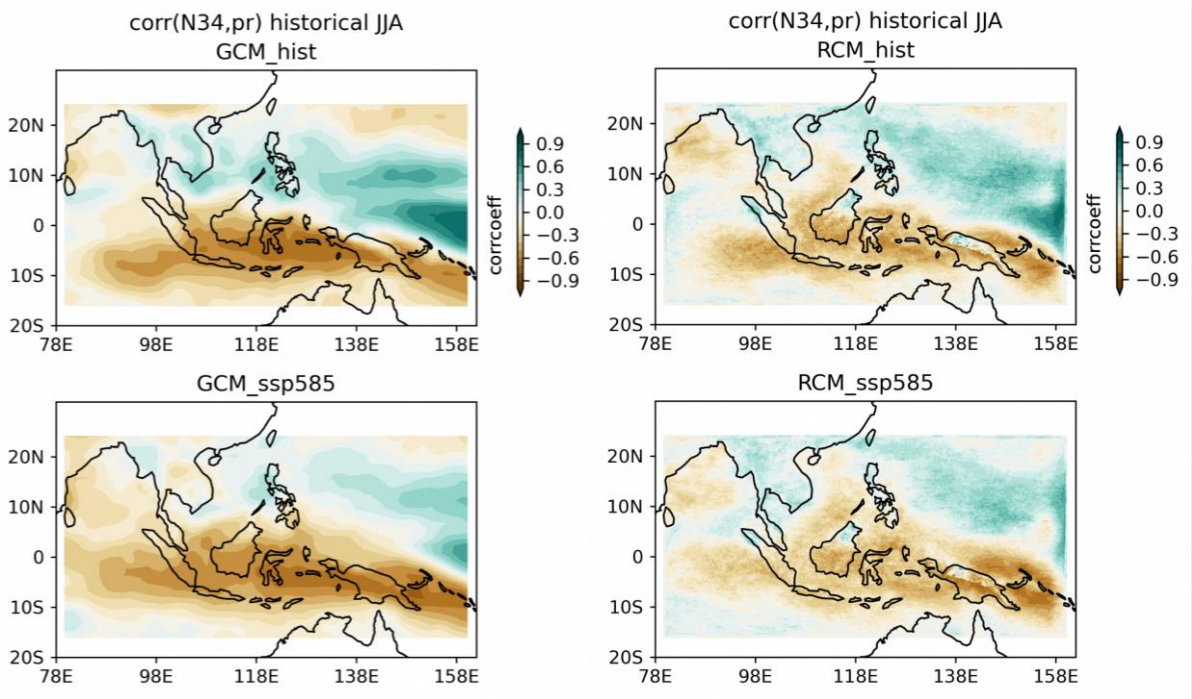

Figure 8.17: JJA ENSO-rainfall teleconnection (correlation coefficient) over the Maritime Continent (left: GCM mean, right: RCM mean. Upper: historical period (1995-2014) . Lower: future (2080-2099) in the SSP585 scenario).

8.5 Summary

This chapter uses projections of 6 CMIP6 GCMs downscaled by SINGV-RCM to examine climate change at regional scales. It examines changes in some important climate variables (e.g. temperature and rainfall). A comparison of the representation of some large-scale drivers are also provided to examine consistency with the GCMs.

Annual-mean domain-average rainfall over SEA is projected to increase both in the mid and end century. While the end-century change projected by the multi-model mean is higher than the mid-century change for each of the scenarios, the magnitude of the inter-model spread can be significant compared to differences in the multi-model mean. The increases noted in the annual mean occur as a result of spatially complex changes in the individual seasons. For example,

there are large percentage increases in climatologically dry periods (e.g. parts of Indochina in DJF and regions around the Java Sea in JJA), and drying over parts of the South China Sea in all seasons.

Extreme rainfall, as quantified by maximum 1-day rainfall (RX1day) and (RX5day), are expected to increase in most of the SEA land regions across the four seasons. Similar to changes in the mean rainfall, some of the largest percentage changes are seen over climatologically dry regions.

As for temperature, multi-model mean projected near-surface air temperatures over the SEA domain are expected to increase by at least 0.8^{o}C in the mid century and by at least 1.0^{o}C in the end century. Based on the multi-model mean projections, SEA land will experience increased warming as compared to the SEA domain by 0.1^{o}C to 0.7^{o}C in the mid-century (Tables 8.7 and 8.8) and up to 4.0^{o}C by the end of the century. This confirms the general expectation from existing studies that the land regions will experience more warming than ocean regions. Changes in annual maximum (tasmax) and annual minimum near-surface air-temperatures are qualitatively similar to those in tas. Based on the multi-model mean, across the seasons, mid-century tasmax would change from 0.9^{o}C-1.7^{o}C while end-century seasonal tasmax would change from 1.0^{o}C-4.1^{o}C.

Similarly, there are widespread increases in temperature extremes, as measured by changes in the seasonal maximum of daily maximum temperatures (TXx) over the SEA domain. The warming is larger over land areas as compared to ocean, exceeding 6^{o}C in parts of Indochina during JJA and SON. In addition, the seasonal minimum of daily minimum temperatures (TNn) increases over much of the domain.

Changes in multi-model seasonal mean near-surface relative humidity (hurs) are either small or negative over land, ranging from 0 to -1.9%, while increases in hurs can be observed over the oceans. Across seasons, the largest decreases can be seen in JJA, especially over Indochina, Borneo, and New Guinea. Similar to the enhanced land warming discussed above, the reduction in relative humidity over land is consistent with findings from existing studies.

Turning to the regional climate drivers, a weakening of the monsoonal flow with anomalous easterlies over the Indian ocean can be seen. Some of the largest changes occur in JJA, where there is also a strengthening of the monsoon flow over Indochina. The changes in the northeast monsoon cold surge are consistent with the GCM changes in terms of increased frequency, anomalous easterlies over Indochina and west of Sumatra, as well as anomalous westerlies north of New Guinea. In contrast, the magnitude of precipitation and rainfall changes in the downscaled simulations are also enhanced relative to the parent GCMs. There are also differences in the details of rainfall: the multimodel mean of the parent GCMs predicts rainfall increase over South Sumatra and Borneo, but the downscaled simulation places the rainfall increase primarily over the Java Sea.

The changes in ENSO teleconnections are consistent with those of the parent GCMs, showing an eastward shift of the zonal dipole pattern such that the negative correlation over the equatorial MC is enlarged while the positive correlation over the eastern MC and Western Pacific are reduced. The downscaled models also offer additional fine-scale spatial details of the ENSO teleconnection.

Overall, the downscaled projections indicate increases in temperature and temperature extremes, as well as rainfall extremes. Annual-mean domain-average rainfall over SEA is projected to increase both in the mid and end century.

Additionally, it's important to highlight the added value of future projections derived from high-resolution RCMs when compared to the coarse-resolution driving GCMs. In the Southeast Asia (SEA) domain, GCMs often exhibit smoothed spatial changes across islands in the equatorial Maritime Continents, attributed to their coarse resolutions at 1.5 degrees latitude/longitude. In contrast, high-resolution (8km) RCMs consistently produce large-scale changes similar to the driving GCMs, offering a more realistic representation of high rainfall variability in the high mountain areas of Java and Papua New Guinea. These enhancements prove crucial for advancing regional climate impact studies.

References

Byrne, M. P., & O'Gorman, P. A. (2018). Trends in continental temperature and humidity directly linked to ocean warming. Proceedings of the National Academy of Sciences, 115(19), 4863–4868. https://doi.org/10.1073/pnas.1722312115

Chen, C., Sahany, S., Moise, A. F., Chua, X. R., Hassim, M. E., Lim, G., & Prasanna, V. (2023). ENSO-rainfall teleconnection over the Maritime Continent enhances and shifts eastward under warming. Journal of Climate, 1(aop), 1–55. https://doi.org/10.1175/JCLI-D-23-0036.1

Tangang, F., Chung, J. X., Juneng, L., Supari, Salimun, E., Ngai, S. T., et al. (2020). Projected future changes in rainfall in Southeast Asia based on CORDEX–SEA multi-model simulations. Climate Dynamics, 55(5–6), 1247–1267. https://doi.org/10.1007/s00382-020-05322-2